RADLAC-II UPGRADE EXPERIMENTS

S. L. Shope, C. A. Frost, D. E. Hasti, G. T. Leifeste,
M. G. Mazarakis, J. W. Poukey, and D. L. Smith
Sandia National Laboratories, Albuquerque, NM 87185

ABSTRACT

The linear induction accelerator, RADLAC II, is being upgraded to produce a 20-MeV, 40-kA annular electron beam with improved beam quality. Previously, the accelerator produced a 15-MeV, 15-kA beam. Improvements in the pulsed power, injector design, and magnetic field have resulted in a faster rising, flat-topped voltage pulse. The first experiments used only the injector and produced a 5.3-MeV, 47-kA high quality annular beam that was transported in a 20-kG magnetic guide field to the location of the first 2.5-MV accelerating gap. The beam is now being transported and accelerated through two of the six accelerating gaps. The accelerating gaps are of a unique design that minimizes changes in the radial electric field to reduce the amplitude of radial oscillations. The quality of the accelerated beam will be measured through two gaps before adding the remainder of the accelerator. Simulations show that the beam quality will be maintained through the accelerator. The final accelerator will produce a 20-MeV, 40-kA annular high quality beam with a small perpendicular velocity component, $v_\perp$, with $\beta_\perp c < 0.2$ c.

INTRODUCTION

The upgrade consists of modifications to the pulsed power and improvements in the injector. Upgrading RADLAC II through straight-forward hardware changes that significantly decrease the inductances and stray capacitances in the water section allows us to attain the upgrade design parameters with good reliability and reproducibility. We learned from the RADLAC-II Module (RIIM) experiments how to improve the pulsed-power performance, and obtained good agreement with circuit modeling analysis.[1] The upgrade is being performed in three steps. The first was installation of the new pulsed power improvements driving only the injector, the second was adding two accelerating stages, and the final step is going to the full accelerator.

RADLAC-II UPGRADE

In the final upgraded accelerator, four Marx generators rather than two, will be used to drive four Hermes-III intermediate storage capacitors (ISC).[2] Each ISC charges two pairs of pulse-forming lines (PFL) through low inductance, low jitter, laser-triggered gas switches developed for PBFA II.[3] The round-trip wave propagation time of each PFL has been increased from 40 to 50 ns. The oil-water interfaces have been relocated to provide symmetrical, low inductance feeds. Figure 1 is a diagram of the upgraded accelerator. The improved geometry and electrical properties of the new pulsed power configuration provide for faster charging times and enables two self-breaking water switches per line to close resulting in a flat-topped voltage pulse in the diodes.

The upgraded RADLAC II will produce a higher current, higher energy, better quality beam. Table 1 shows the comparison between the previous beam parameters and the predicted parameters for the upgraded accelerator, based on measured injector performance.

Table I. Comparison of RADLAC-II beam parameters.

Parameter	Before Upgrade	After Upgrade
Energy ($(\gamma-1)mc^2$)	14 MeV (1.75 MV/stage)	20 MeV (2.5 MV/stage)
Current (I)	18 kA	42 kA
Beam Radius (r)	1.4 cm	0.9 cm
Perpendicular Thermal Velocity ($\beta_\perp c$)	0.16 c	0.05 c
Normalized Emittance Including Rotation (ε_n)	7.5 rad-cm	5.9 rad-cm
Brightness (B_n)	33 A/(rad-cm)^2	123 A/(rad-cm)^2

Parameters from before the upgrade are based on measured output from the accelerator. Parameters for the upgraded beam are based on particle code predictions of accelerator performance using measured input beam parameters from the first step injector experiments. The normalized emittance, ε_n, is defined as[4]

$$\varepsilon_n = \sqrt{(\gamma r \beta_\perp)^2 + (P_\theta/c)^2}\ ,$$

$$\text{where } (P_\theta/c) = \frac{1}{2}\frac{1}{mc^2} r_k^2 B_k$$

in the accelerator magnetic guide field, r_k and B_k are the cathode radius and magnetic guide field at the cathode, and $(P_\theta/c) = r\gamma\beta_\theta$ after extraction for the magnetic guide field. The brightness is defined as[5]

$$B_n = \frac{I}{(\pi\varepsilon_n)^2}\ .$$

Figure 2 shows a measured voltage waveform for one diode driven by an upgraded pulsed power module compared to a diode voltage waveform before the upgrade. This demonstrates the 2.5 MV per stage and waveform requirements.

CIRCUIT SIMULATIONS

The circuit model simulated with the SCEPTRE network solving code employs several transmission line models to account for the proper locations and dimensions of the hardware.[6] Careful attention was given to accurately represent all of the feed line inductances and stray capacitances, as well as the major components. All components and sections were modeled with the JASON electrostatic field code to identify the effective capacitances and the best field grading geometries.[7] The primary model represents one quarter of the accelerator and includes a Marx generator, one ISC, one gas switch, four PFLs and their eight output water switches, four convolute sections, and a common, mismatched (1.28:1), resistive load. To account for the leakage to fringing fields in the water around the vacuum insulator stacks, a parallel load shunt resistance (16 ohms per line) was

estimated by simple circuit analysis and RIIM accelerator data and included in the model through the load mismatch. The parallel PFLs and convolutes are lumped together to form a series train of transmission lines for convenience. The switch models are represented by a series combination of exponentially time-varying resistor and appropriate inductor with both shunted by a parallel stray capacitance.

The power pulse that progresses through the model begins with a 3.2-MV erected Marx generator, corresponding to an initial charging voltage of 80 kV. This Marx charge voltage allows operation of the accelerator with reliability corresponding to a safety factor of 20% or better with respect to the breakdown fields in water or along the insulators. The ISC has a peak voltage of 2.7 MV before the gas switch closes. A 300-kA peak current passes through the gas switch. The PFLs charge to a peak voltage of 2.7 MV when the water switches close and transfer the short pulse down the output transmission lines along the convolute sections. Each water switch gap conducts a peak current of 125 kA. The experimental results favorably compare with the waveforms generated by the model as shown in Fig. 3.

INJECTOR EXPERIMENTS

The first experiments used one Marx generator and ISC to drive the injector. The injector consists of two vacuum diodes in series that contain the anode and cathode. Time-integrated pinhole photographs of the previous injector geometry showed the beam was large and had a halo that was approximately the same diameter as the drift tube, see Fig. 4a. Particle simulations for this geometry indicated there was a large loss of shank current (60%) due to the loss of magnetic insulation. The front surface of the cathode shank was also emitting electrons, some of which were getting into the drift pipe and causing the large diameter beam.

The shank diameter was reduced from the original 20 cm to 1.3 cm to reduce spurious electron emission. A 2-cm diameter, 5.3-MeV, 47-kA annular beam was produced with this geometry. These current levels are consistent with the space charge limited current predicted by analytic theory. The space charge limited current is given by[8]:

$$I_{anal} = (1-0.3\,L^{*})(\gamma^{2/3} - 1)^{3/2}\ (17\ kA)\ \frac{r_b}{\delta}\left[\ln\left(\frac{8\delta}{a}\right)\right]^{-1},$$

$$\gamma = \frac{V(MV)}{.511} + 1,\quad L^{*} = \text{Dimensionless number equal to the anode-cathode gap in cm},$$

$$r_b = \frac{r_1 + r_2}{2},\quad \delta = R - r_2,\quad a = r_2 - r_1.$$

For the RADLAC injector, r_1 = 0.7 cm, r_2 = 1.0 cm, R = 1.6 cm, and L = 1.0 cm. A comparison of the predicted current and measured current along with our geometry is shown in Fig. 5.

Figure 4b is an x-ray pinhole photograph of the beam. The $\beta_\perp$ for this beam was 0.16. The perpendicular velocity can be calculated directly from measurements of a time-integrated x-ray pinhole photograph. The width of the annulus is a function of the cathode dimensions, the applied magnetic field, the beam energy and camera geometry. These are known quantities and can be used to calculate $\beta_\perp$ from Larmor radius effects.[9] The smaller diameter shank increased the inductance of the injector and was also difficult to keep in alignment. A new shank was designed taking magnetic insulation, inductance and mechanical stability into consideration. The new shank is 10 cm in diameter and tapers to the cathode diameter. The new design has also produced a 2-cm diameter annular beam with a $\beta_\perp$ of 0.10. The new cathode is easy to align and has remained aligned for at least 50 shots. The injector is described in detail by Mazarakis et al.[10]

New magnetic guide coils were also installed and resulted in a more uniform magnetic field in the foilless diode region and across the accelerating gaps. The non-uniformities have been reduced from 40% to ~10%. They are also designed to produce 20 to 25-kG fields rather than the 12 to 16-kG fields of the old coils. The improved magnetic field will minimize beam expansion due to field variations.

ACCELERATION EXPERIMENTS

An additional Marx generator and the associated pulsed power hardware has been added to drive two acceleration modules. The additional gas switch requires laser-triggering for pulse simultaneity better than 10 ns. Each accelerating stage consists of a vacuum diode containing contoured accelerating gaps that were designed to minimize radial oscillations of the electron beam.[11] Experiments are currently in progress to measure the beam parameters after acceleration through two stages.

CONCLUSIONS

We have developed an injector that produces a 5-MeV, 40-kA high quality annular beam that meets the requirements for meaningful propagation experiments. The beam is being accelerated and measurements of the beam are being made. Simulations and experiments indicate the full accelerator will produce a 20-MeV, 40-kA annular beam with a $\beta_\perp < 0.2$.

ACKNOWLEDGEMENTS

The authors would like to thank the RADLAC-II technicians: Dennis Bolton, Tom Coffman, Janet Finch, Mike Harden, and Chip Olson. Their efforts have contributed to the success of the experiments. This work was funded by the U.S. DOE under contract DE-AC04-76DP00789, DARPA/AFWL under ARPA Order 5789, DARPA/NSWC. under ARPA Order 4395.

REFERENCES

1. D. L. Smith et al., SNLA SAND88-1158, Albuq., NM, 1988.
2. J. J. Ramirez et al., "The HERMES-III Program," Proc. of the 6th IEEE Pulsed Power Conf., (Arlington, VA, June 1987), IEEE Cat. No. 87CH2522-1, p. 294.
3. D. R. Humphreys et al., "RIMFIRE, A Six Megavolt Laser-Triggered Gas-Filled Switch for PBFA II," Proc. 5th IEEE Pulsed Power Conf., (Arlington, VA, June 1985), IEEE Cat. No. 85C2121-2, p. 262.
4. E. P. Lee and R. K. Cooper, Particle Accelerator 7, 83, 1976.
5. T. C. Marshall, Free Electron Lasers, MacMillan Publishing Company, New York, 1985, p. 103.
6. J. C. Bowers and S. R. Sedore, SCEPTRE: A Computer Program for Circuit and System Analysis, Englewood Cliffs, NJ, Prentice Hall, 1971.
7. S. J. Sackett, "JASON - A Code for Solving General Electrostatics Problems, User's Manual, LLL CID-17814, Livermore, CA, 1978.
8. E. Ott et al., Lovelace, Phys. Fluids 20, 1180 (1977).
9. D. E. Hasti et al., "RADLAC-II Upgrade Injector Experiments," SNLA SAND88-1032, Albuq., NM, 1988.
10. M. G. Mazarakis et al., RADLAC-II Injector Designs," this conference.
11. S. L. Shope et al, "The Design of the Accelerating Gaps for the Linear Induction Accelerator RADLAC II," Proc. 1987 IEEE Particle Accelerator Conf., (Washington, DC, March 16-19, 1987), p. 978.

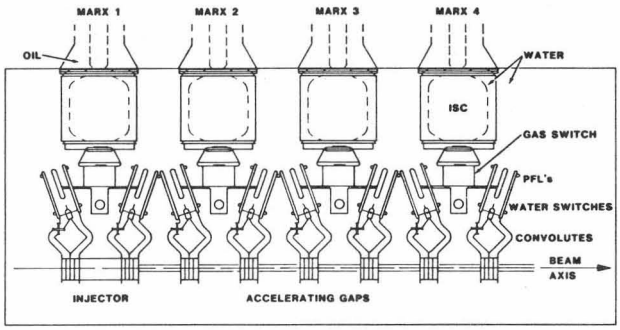

Fig. 1. Top view of water tank hardware layout. There is another set of PFLs, water switches and convolutes under those shown.

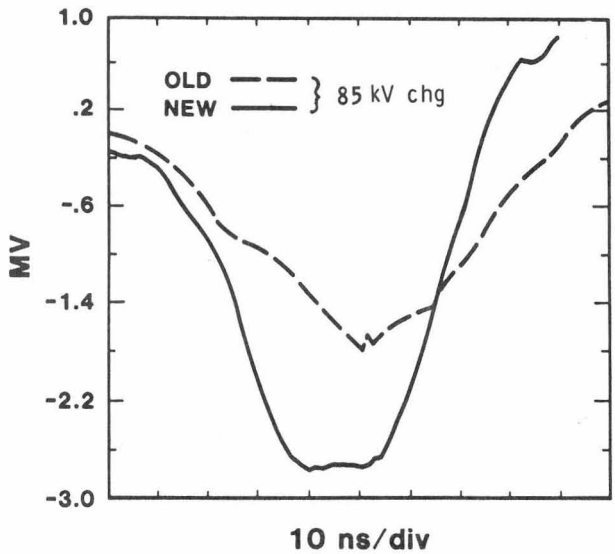

Fig. 2. Comparison of voltage waveforms of a single injector module of the old and new configuration.

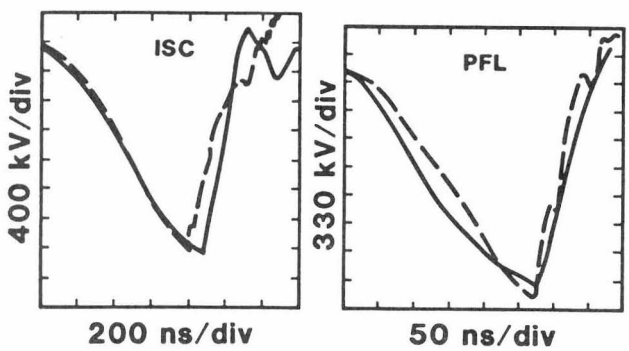

Fig. 3. Comparison of measured (solid lines) and simulated voltage waveforms.

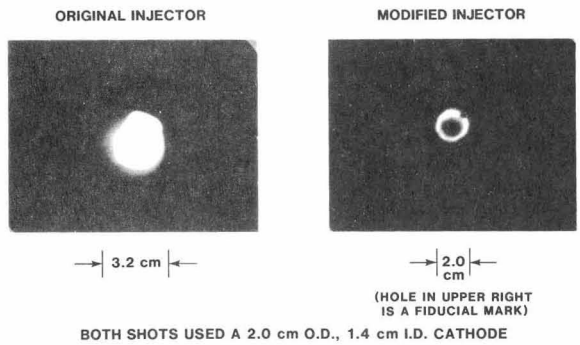

Fig. 4. Figure a is a x-ray pinhole of the old injector. Figure b is the new injector.

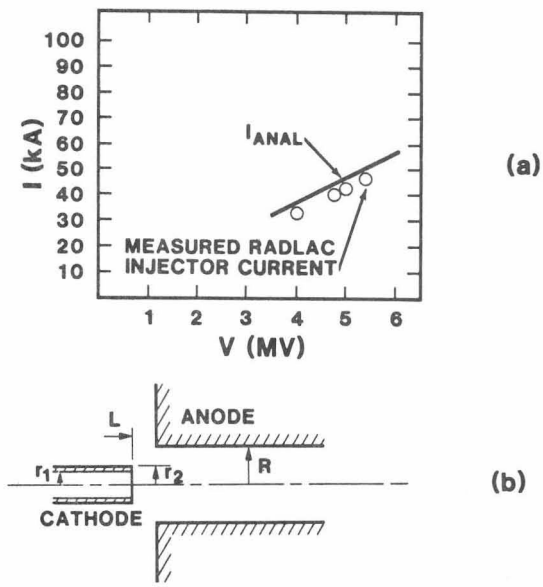

Fig. 5. Comparison of analytical and experimental currents is shown in part a. The geometry is shown in part b.